Thermal processes in the oscillations of gas bubbles in tubes

X. M. Chen and A. Prosperetti

Department of Mechanical Engineering, The Johns Hopkins University, Baltimore, Maryland 21218

The forced oscillations of a system consisting of two finite liquid columns in a duct separated by a gas bubble are studied in the linear approximation. It is found that thermal processes in the gas induce a very significant damping in the system, which can exceed viscous damping even in capillaries with a submillimeter diameter. The study is motivated by the possibility of using gas bubbles as actuators in microdevices. © *1998 Acoustical Society of America.*
[S0001-4966(98)00608-0]

PACS numbers: 43.35.Ud [HEB]

INTRODUCTION

It is well known that a gas bubble pulsating in a large liquid mass loses energy by viscosity, acoustic radiation, and thermal conduction (see, e.g., Apfel, 1981; Prosperetti, 1984, 1991). The additional dissipation due to gas diffusion is essentially always negligible, while thermal effects due to phase change are insignificant for a liquid like water at normal temperature. Over a wide range of bubble radii and frequencies, thermal conduction is by far the most significant dissipative mechanism. In addition to energy dissipation, thermal processes also influence the stiffness of the bubble the behavior of which, in general, will be intermediate between isothermal and adiabatic. The corresponding processes for bubbles pulsating in a duct have not been studied, and they constitute the object of this paper.

The motivation for this work lies in the possibility to use pulsating bubbles as actuators in small fluid-handling devices such as those made possible by recent progress in silicon manufacturing techniques (see e.g., Fujita and Gabriel, 1991; Lin and Pisano, 1991; Gravesen *et al.*, 1993). Of course, energy dissipation is important as it determines the width of the resonance and the magnitude of the response under forced oscillation. The stiffness of the bubble determines the resonance frequency.

I. FORMULATION

Since this is the first study devoted to the problem, we feel justified in introducing some approximations that will, on the one hand, simplify the analysis and, on the other, facilitate a comparison with the established results for a spherical bubble.

In the first place, and just as in the case of a spherical bubble, we assume the wavelength in the gas to be much larger than both the lateral dimensions of the channel and the axial length of the bubble, so that the gas pressure can be considered spatially uniform and only a function of time (see, e.g., Prosperetti, 1991). Another approximation in common with the standard analyses for spherical bubbles is the neglect of the vapor contribution to the bubble internal pressure and of phase change processes, both approximations being motivated by the consideration of only relatively ''cold'' liquids (see, e.g., Plesset and Prosperetti, 1977).

In the case of bubbles in large liquid masses a substantial simplification arises from the assumption of spherical shape. Here we introduce a parallel assumption on the shape of the bubble: since our interest lies in channels with a diameter of the order of 1 mm or less, we take the bubble to occupy an entire section of the channel, ignoring the problems associated with contact angles and the detailed shape of the gas-liquid interface (Fig. 1). The gas volume is therefore assumed to be bounded by two flat liquid surfaces orthogonal to the axis of the channel, and by the surface of the channel comprised between these two surfaces. The amplitude of the oscillations is taken to be so small that the problem can be linearized, and the liquid surfaces bounding the gas volume are supposed to move remaining flat and orthogonal to the channel walls; the complexities associated with the motion of the gas–liquid–solid contact line are therefore ignored. This approximation has the consequence of rendering it impossible to account for a velocity profile in the liquid. Energy dissipation due to liquid viscosity will be reintroduced in an approximate way later (Sec. V). In spite of the relative crudeness of this model, one may expect the results to be a valid first estimate of the quantitative effects of the physical processes involved.

Let $x_1(t)$ and $x_2(t)$ denote the time-dependent positions of the two gas–liquid interfaces, both measured from the midpoint of the undisturbed bubble, and define

$$x_2 - x_1 = 2L_B[1 + X(t)], \tag{1}$$

where $2L_B$ is the undisturbed length of the bubble. We shall only consider the steady-state problem in which the time dependence of all disturbances is proportional to $\exp i\omega t$.

Due to the translational invariance of the channel and to the fact that, in a linear problem, the perturbation of any quantity is proportional to that of any other, one may write without loss of generality the gas pressure in the form

$$p(t) = p_0[1 - \Phi X(t)], \tag{2}$$

where p_0 is the equilibrium value and Φ is a complex constant. It will be noted that this relation may be considered as the linearization of a relation of the type $pV^\Phi = \mathrm{const}$ (where V is the bubble volume), so that Φ may be regarded as a (complex, frequency dependent) polytropic index.
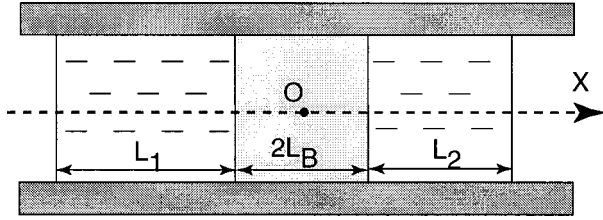
FIG. 1. The physical model simulated in this study: a duct contains two liquid columns separated by a gas bubble.

If the length of the liquid columns bounded by the surface x_j, $j=1,2$, is denoted by L_j, and if the pressure acting on the free end of each column is

$$p_j(t) = p_0[1 + P_j(t)], \tag{3}$$

the equations of motion for the columns are

$$L_1 \rho \ddot{x}_1 = p_0[P_1 + \Phi X], \tag{4}$$

$$L_2 \rho \ddot{x}_2 = -p_0[P_2 + \Phi X], \tag{5}$$

where ρ is the liquid density. Define the abscissa of the center of mass of the liquid by

$$\xi = \frac{L_1 x_1 + L_2 x_2}{L_1 + L_2} + \frac{1}{2}(L_2 - L_1). \tag{6}$$

Then the two equations can be combined to give equations of motion for ξ and X:

$$\rho(L_1 + L_2)\ddot{\xi} = p_0(P_1 - P_2), \tag{7}$$

$$\ddot{X} = -\frac{p_0}{2L_B \rho}\left[\frac{1}{L_2}(P_2 + \Phi X) + \frac{1}{L_1}(P_1 + \Phi X)\right]. \tag{8}$$

Upon noting that $iX = \dot{X}/\omega$, the second equation may be rewritten as

$$\ddot{X} + \frac{p_0}{2L_B\rho\omega}(\text{Im }\Phi)\left[\frac{1}{L_1} + \frac{1}{L_2}\right]\dot{X} + \frac{p_0}{2L_B\rho}(\text{Re }\Phi)\left[\frac{1}{L_1} + \frac{1}{L_2}\right]X$$

$$= -\frac{p_0}{2L_B\rho}\left[\frac{P_1}{L_1} + \frac{P_2}{L_2}\right]. \tag{9}$$

The equation for ξ describes the overall motion of the system. In particular, if $P_1 = P_2$ and the initial velocity vanishes, ξ is independent of time irrespective of the behavior of the bubble. Thermal effects only affect the second equation (8) through Φ, and it is on this quantity that we now focus. It is obvious from (9) that the real part of this quantity governs the natural frequency of the system, while the imaginary part is responsible for thermal dissipation.

The determination of Φ requires a consideration of the energy equation. For a perfect gas with spatially uniform pressure p, in the linear approximation, this is

$$\rho_G c_p \frac{\partial T}{\partial t} - \dot{p} = k\nabla^2 T, \tag{10}$$

where T is the gas temperature, ρ_G is its density, c_p is the specific heat at constant pressure, and k is the thermal conductivity. By combining with the equation of continuity and using the relation $c_p \rho_G T_0 = \gamma p_0/(\gamma - 1)$ valid for perfect

gases (with γ the ratio of specific heats), this equation becomes

$$\dot{p} - \gamma p \nabla \cdot \mathbf{u} = k\nabla^2 T, \tag{11}$$

where $\mathbf{u}$ is the gas velocity. When this equation is integrated over the surface of the gas volume V one finds an equation for the gas pressure in the form

$$V\dot{p} = -\gamma p\dot{V} - (\gamma - 1)Q, \tag{12}$$

where

$$Q = -\oint_A k \frac{\partial T}{\partial n} dA \tag{13}$$

is the total heat flow rate out of the surface A bounding the bubble. The calculation of the gas pressure presupposes a knowledge of Q, and hence of the gas temperature field, to which we now turn.

II. THE THERMAL PROBLEM

By virtue of the assumed exponential time dependence, the energy equation (10) may be written

$$\left(\nabla_\perp^2 + \frac{\partial^2}{\partial x^2}\right)T - i\frac{\omega}{D}(T - T_0) = i\frac{\gamma - 1}{\gamma}\frac{\omega}{D}T_0\Phi X, \tag{14}$$

where $D = k/\rho_G c_p$ is the gas thermal diffusivity, T_0 is the undisturbed temperature of the system, and $\nabla_\perp^2$ denotes the two-dimensional Laplacian over the cross section of the channel, the shape of which for the moment we do not need to specify. At this point we introduce another assumption which is also standard for a gas bubble in a large mass of liquid, namely that the surface delimiting the gas remains at the undisturbed temperature T_0. The justification for this assumption lies in the large heat capacity *per unit volume* of most solids and liquids, which far exceeds that of gases. Amounts of heat sufficient to cause significant temperature changes in the gas are therefore too small to cause any appreciable temperature disturbance in the materials surrounding the bubble. On this basis, we seek a solution of (14) subject to the condition $T = T_0$ on the boundary of the gas volume.

We determine this solution by expanding T over a set of eigenfunctions of $\nabla_\perp^2$. Specifically, consider the eigenfunction, eigenvalue pairs (v_n, λ_n) satisfying

$$\nabla_\perp^2 v_n = -\frac{\lambda_n^2}{l^2} v_n, \tag{15}$$

over the cross section of the channel, subject to the boundary condition $v_n = 0$ on the perimeter of the cross section. Depending on the shape of the cross section, the index n may actually stand for a pair of indices, as in one of the examples of Sec. IV below. In (15) we have made the eigenvalues dimensionless in terms of a characteristic length l defined as the ratio of the bubble volume to its surface:

$$l = \frac{L_B S}{S + \mathscr{P} L_B}, \tag{16}$$

where S is the area of the cross section and $\mathscr{P}$ is its perimeter. The reason for this definition is the fact that, when one

of the lengths characterizing the geometry of the bubble (e.g., its extension in the axial direction, or the size of the channel cross section) is much smaller than the others, l is close to this length. Thus, l is a measure of the shortest distance between the bubble "core" and the fixed-temperature boundaries that enclose the gas. The physical relevance of this distance will be apparent shortly.

It is easy to see, by use of Green's identity, that the eigenfunctions satisfying (15) are orthogonal to each other (see the Appendix). We thus write

$$T = T_0 \left[1 + \sum_n A_n(x,t) v_n(y,z) \right], \tag{17}$$

substitute into (14), and exploit the orthogonality of the eigenfunctions to find

$$\frac{\partial^2 A_n}{\partial x^2} - \frac{k_n^2}{l^2} A_n = i \frac{\gamma-1}{\gamma} \frac{\omega \sqrt{S}}{D} \sigma_n \Phi X, \tag{18}$$

where

$$k_n = \sqrt{\lambda_n^2 + i\Omega}, \quad \Omega = \frac{\omega l^2}{D}, \tag{19}$$

$$\sigma_n = \frac{1}{\sqrt{S}} \int_S v_n \, dS. \tag{20}$$

Due to linearization, the boundary conditions are $A_n = 0$ at the undisturbed positions $x_{i0} = \mp L_B$, $i=1,2$, of the liquid surfaces bounding the bubble. The solution is readily found to be

$$A_n = i \frac{\gamma-1}{\gamma} \frac{\omega l^2 \sqrt{S}}{D} \frac{\sigma_n}{k_n^2} \left[\frac{\cosh k_n x/l}{\cosh k_n L_B/l} - 1 \right] \Phi X, \tag{21}$$

where it will be recalled that the coordinate x is measured from the midpoint of the undisturbed bubble.

With this result the heat flow rate Q can be calculated from (13). We break up the integral into the contribution Q_s of the liquid surface and the contribution Q_w of the tube wall, $Q = Q_s + Q_w$. For the former we have

$$Q_s = -2k \int_S \left. \frac{\partial T}{\partial x} \right|_{x=L_B} dS$$

$$= i\omega(p-p_0)V \sum_n \sigma_n^2 \frac{\tanh k_n \mathscr{A}}{k_n \mathscr{A}}, \tag{22}$$

where $\mathscr{A}$ is the *aspect ratio* of the bubble defined by

$$\mathscr{A} \equiv \frac{L_B}{l} = 1 + \frac{4L_B}{\mathscr{D}}, \tag{23}$$

with $\mathscr{D} = 4S/\mathscr{P}$ the hydraulic diameter of the tube. For the second component we have, noting that $\mathbf{n} \cdot \nabla = \mathbf{n} \cdot \nabla_\perp$,

$$Q_w = -2kT_0 \sum_n \int_0^{L_B} A_n \, dx \int_{\mathscr{P}} d\mathscr{P} \, \mathbf{n} \cdot \nabla_\perp v_n$$

$$= -2kT_0 \sum_n \int_0^{L_B} A_n \, dx \int_S dS \, \nabla_\perp^2 v_n$$

$$= -2kT_0 \sum_n \int_0^{L_B} A_n \, dx \int_S dS \left(-\frac{\lambda_n^2}{l^2} \right) v_n$$

$$= i\omega(p-p_0)V \sum_n \frac{\sigma_n^2 \lambda_n^2}{k_n^2} \left(1 - \frac{\tanh k_n \mathscr{A}}{k_n \mathscr{A}} \right), \tag{24}$$

where in the first step we have used the divergence theorem to convert the line integral over the perimeter of the cross section into a surface integral over the cross section, and in the following steps the eigenvalue equation (15) and the definition (20) of σ_n. Upon combining the two contributions (22) and (24) we then find

$$Q = i\omega(p-p_0)VG, \tag{25}$$

where

$$G = \sum_n \frac{\sigma_n^2}{k_n^2} \left[\lambda_n^2 + i\Omega \frac{\tanh k_n \mathscr{A}}{k_n \mathscr{A}} \right]. \tag{26}$$

Upon substitution of (25) into the pressure equation (12) we find, comparing with (2),

$$\Phi = \frac{\gamma}{1 + (\gamma-1)G}. \tag{27}$$

In the framework of the present model, the function G describes the effect of the thermal processes occurring in the bubble on the gas pressure. An alternative form for this quantity may be derived by using the identity

$$\sum_n \sigma_n^2 = 1, \tag{28}$$

proven in the Appendix, to obtain

$$G = 1 + i\Omega \sum_n \left(\frac{\sigma_n}{k_n} \right)^2 \left[\frac{\tanh k_n \mathscr{A}}{k_n \mathscr{A}} - 1 \right]. \tag{29}$$

Since G is complex, Eq. (25) shows that the heat transfer rate has components in phase and in quadrature with the pressure disturbance. The former one is proportional to Im G, and is responsible for the thermal losses of the system. Although it might seem that G depends explicitly only on Ω and $\mathscr{A}$, there may be an additional dependence on other dimensionless parameters characterizing the shape of the tube cross section through the eigenvalues λ_n.

III. ASYMPTOTIC BEHAVIOR

Before looking at numerical results for some specific examples, it is useful to consider two limit cases of the previous results (26) and (27) that are applicable to channels of arbitrary cross section.

We start with the low-frequency limit or, more precisely, with frequencies such that the corresponding thermal penetration length is much larger than the smallest bubble dimension:

$$\sqrt{\frac{D}{\omega}} \gg l. \tag{30}$$

In these conditions the parameter Ω, defined in (19), is small, and one would expect nearly isothermal behavior to prevail. To confirm this expectation we approximate the expression (19) for k_n and the hyperbolic tangent in (29) by a Taylor series and find

$$G = 1 + \Omega^2 \sum_n \frac{\sigma_n^2}{\lambda_n^4} \left[\frac{3}{2} \frac{\tanh \lambda_n \mathscr{A}}{\lambda_n \mathscr{A}} - \frac{1}{2 \cosh^2 \lambda_n \mathscr{A}} - 1 \right]$$
$$+ i\Omega \sum_n \frac{\sigma_n^2}{\lambda_n^2} \left(\frac{\tanh \lambda_n \mathscr{A}}{\lambda_n \mathscr{A}} - 1 \right), \tag{31}$$

from which

$$\mathrm{Re}\ \Phi = 1 + \frac{\gamma-1}{\gamma} \Omega^2 \sum_n \frac{\sigma_n^2}{\lambda_n^4} \left[\frac{3}{2} \frac{\tanh \lambda_n \mathscr{A}}{\lambda_n \mathscr{A}} \right.$$
$$\left. - \frac{1}{2 \cosh^2 \lambda_n \mathscr{A}} - 1 + \cdots \right], \tag{32}$$

$$\mathrm{Im}\ \Phi = \frac{\gamma-1}{\gamma} \Omega \sum_n \frac{\sigma_n^2}{\lambda_n^2} \left[1 - \frac{\tanh \lambda_n \mathscr{A}}{\lambda_n \mathscr{A}} + \cdots \right]. \tag{33}$$

These formulas simplify if $\mathscr{A} = L_B/l \gg 1$, i.e., for a relatively long bubble. In this case they become

$$\mathrm{Re}\ \Phi \simeq 1 + \frac{\gamma-1}{\gamma} \Omega^2 \sum_n \frac{\sigma_n^2}{\lambda_n^4} \left[\frac{3}{2} \frac{1}{\lambda_n \mathscr{A}} - 1 \right], \tag{34}$$

$$\mathrm{Im}\ \Phi \simeq \frac{\gamma-1}{\gamma} \Omega \sum_n \frac{\sigma_n^2}{\lambda_n^2} \left[1 - \frac{1}{\lambda_n \mathscr{A}} \right]. \tag{35}$$

A parallel analysis of the opposite limit of large Ω is complicated mathematically although, of course, one expects an adiabatic behavior for which $\Phi \to \gamma$. Rather than starting from the explicit representations (26) or (29), it is simpler to proceed as follows. Consider a one-dimensional problem in which a constant-temperature plane surface is exposed to a gas environment of infinite extent, the pressure of which fluctuates in time. One readily finds the following result for the heat flux out of the gas volume:

$$q = -(p-p_0)\sqrt{i\omega D}. \tag{36}$$

In the high-frequency limit, when the thermal penetration layer in the gas is much smaller than the geometric dimensions of the bubble, each point at the bubble surface is subject to this heat flux, so that the total heat transfer rate out of the gas volume must become, for $\omega \to \infty$,

$$Q \simeq 2(L_B\mathscr{P}+S)(p-p_0)\sqrt{i\omega D}. \tag{37}$$

Upon equating to the previous general result (25) for Q, we find

$$G \to \frac{1-i}{\sqrt{2\Omega}} \quad \text{for } \Omega \to \infty, \tag{38}$$

from which we have the following asymptotic limits:

$$\mathrm{Re}\ \Phi \to \gamma \left[1 + \frac{\gamma-1}{\sqrt{2\Omega}} \right], \quad \mathrm{Im}\ \Phi \to \frac{\gamma(\gamma-1)}{\sqrt{2\Omega}}. \tag{39}$$

It will be observed that these results are independent of the aspect ratio $\mathscr{A}$, a result that it would be quite difficult to establish directly from (26) or (29).

By following a similar line of approach we can deduce approximate results valid for very short bubbles, $\mathscr{A}-1 \ll 1$, and very long bubbles, $\mathscr{A} \gg 1$. In the former case most of the heat exchange occurs with the liquid and one can ignore the directions orthogonal to the duct axis. Upon dropping the operator $\nabla_\perp^2$ in the energy equation (14) we find

$$T - T_0 = \frac{D}{k}(p-p_0)\left(1 - \frac{\cosh\sqrt{i\omega/D}x}{\cosh\sqrt{i\omega/D}L_B} \right), \tag{40}$$

from which the total heat flow rate into the liquid is readily found as

$$Q = 2S(p-p_0)\sqrt{i\omega D}\ \tanh(\sqrt{i\Omega}\mathscr{A}). \tag{41}$$

Upon comparison with (25) we thus have

$$G \simeq \frac{\tanh(\mathscr{A}\sqrt{i\Omega})}{\mathscr{A}\sqrt{i\Omega}}, \quad \mathscr{A} \to 1. \tag{42}$$

It is readily checked that this result agrees with (31) for small Ω, and, noting that $\mathscr{A} \simeq 1$, with (38) for large Ω. The real and imaginary parts of Φ evaluated using G given by (42) are plotted in Fig. 2(a) and (b) as functions of $\Omega \mathscr{A}^2$. These results are valid whatever the shape of the cross section of the duct.

For the opposite limit of a long bubble, heat exchange occurs mostly with the wall of the tube and the x derivative in (14) can be dropped. The temperature field can be solved by using the same expansion (17) as before in which, however, the coefficients A_n are constants. Other than this change, the calculation is therefore the same as the general one outlined in the previous section and one finds

$$G \simeq \sum_n \frac{\sigma_n^2 \lambda_n^2}{\lambda_n^2 + i\Omega}. \tag{43}$$

It will be observed that this is just the first summation in (26). For Ω small we recover (31) to first order.

IV. SPECIFIC EXAMPLES

The limits considered in the previous section appear to be the only ones for which results valid for arbitrary cross sections can be derived. For intermediate values of the frequency, we need to consider specific geometries. As noted before, for each specific shape of the cross section of the tube, the result (26) depends on the dimensionless frequency Ω defined by (19), the aspect ratio $\mathscr{A}$ defined by (23), and possibly other dimensionless parameters characterizing the shape of the cross section.

A. Circular tube

For a circular tube of radius R, the characteristic length l defined by (16) is given by
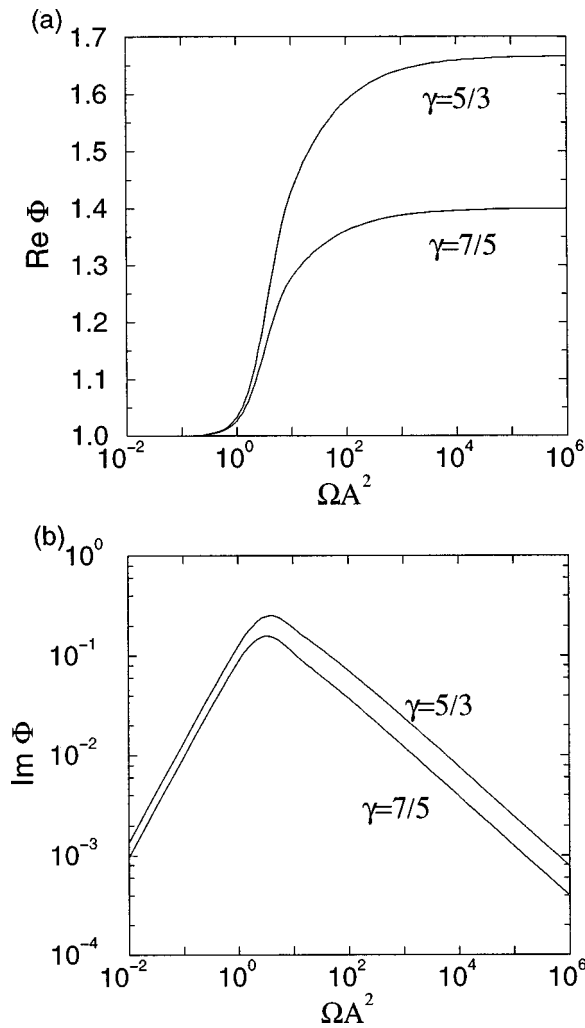
FIG. 2. The real (a) and imaginary (b) parts of Φ evaluated using the approximate result (42) valid for short bubbles as functions of the $\Omega\mathscr{A}^2$, where Ω is the dimensionless frequency given by (19) and $\mathscr{A}$ is the aspect ratio (23). These results are valid for any shape of the cross section of the duct.
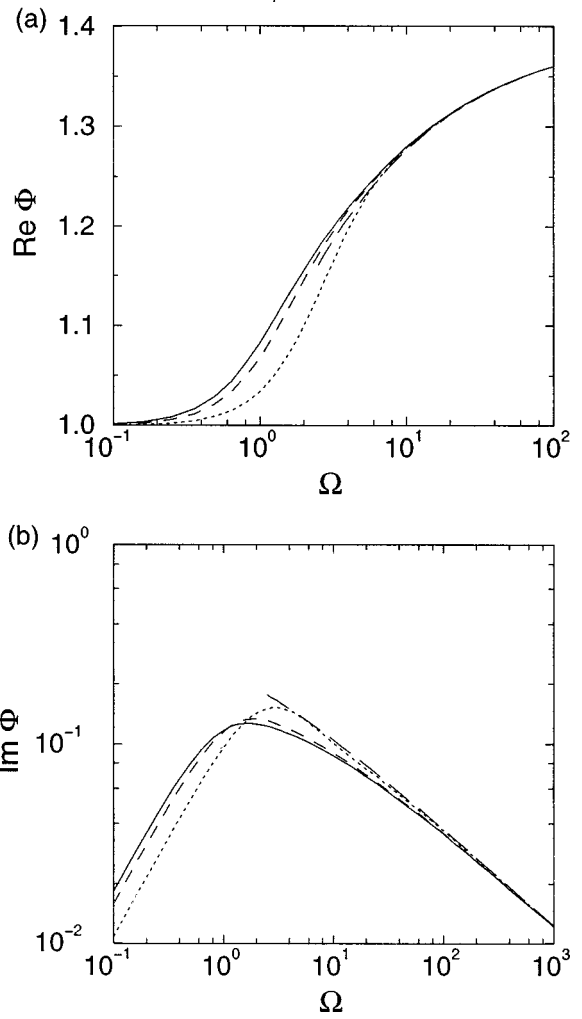
FIG. 3. The real (a) and imaginary (b) parts of Φ as functions of the dimensionless frequency Ω defined in (19) for $\gamma=7/5$ for a cylindrical cross section. The three lines correspond to $\mathscr{A}=1.1$ (dotted), 2 (solid), and 11 (dashes), i.e., to $2L_B/R=0.1$, 1, and 10, respectively. The interrupted line marked with long dashes is the asymptotic approximation (39) valid at high frequencies.

$$l=\frac{RL_B}{R+2L_B},\tag{44}$$

so that the aspect ratio is

$$\mathscr{A}=1+\frac{2L_B}{R}.\tag{45}$$

The eigenfunctions, normalized according to (A4) of the Appendix, are given by

$$v_n=\frac{1}{\sqrt{\pi}R}\frac{J_0(\alpha_n r/R)}{J_1(\alpha_n)},\tag{46}$$

where r is the radial distance from the tube axis, the J's are Bessel functions, and the α_n's are the zeros of $J_0'=-J_1$. The eigenvalues λ_n are given by

$$\lambda_n=\alpha_n\frac{l}{R}=\alpha_n\frac{\mathscr{A}-1}{2\mathscr{A}},\tag{47}$$

which shows that, for this geometry, the function G only depends on $\mathscr{A}$ and Ω. The constants σ_n defined in (20) are readily calculated and they are

$$\sigma_n=\frac{2}{\alpha_n}.\tag{48}$$

With these results, the function Φ can be calculated explicitly as a function of the parameters of the problem. We show in Fig. 3 the real and imaginary parts of Φ as functions of the dimensionless frequency Ω for $\gamma=7/5$. The three lines correspond to $\mathscr{A}=1.1$ (dotted), 2 (solid), and 11 (dashed), i.e., to $2L_B/R=0.1$, 1, and 10, respectively. The asymptotic trends for small and large frequencies are in precise agreement with the deductions of the previous section. The lines for $\mathscr{A}=1.1$ are nearly identical to the approximation shown in Fig. 2.

The figures also show that the results are close to each other, and their variation with the parameter $\mathscr{A}$ is not systematic. Both features indicate that the characteristic length l

defined in (16) is effective in achieving an approximate scaling for Φ.

B. Rectangular channel

For a rectangular cross section of sides a and b the eigenfunctions are labelled by a pair of indices and are given by

$$v_{nm} = \frac{2}{\sqrt{ab}} \sin \frac{m\pi y}{a} \sin \frac{n\pi z}{b}. \tag{49}$$

The characteristic length l of (16) and aspect ratio $\mathcal{A}$ of (23) are

$$l = \frac{abL_B}{ab + 2(a+b)L_B}, \quad \mathcal{A} = 1 + \frac{2L_B(a+b)}{ab}, \tag{50}$$

the eigenvalues are

$$\frac{\lambda_{nm}}{l} = \pi \left[\left(\frac{m}{a} \right)^2 + \left(\frac{n}{b} \right)^2 \right]^{1/2}, \tag{51}$$

and

$$\sigma_{nm} = \frac{8}{mn\pi^2}, \tag{52}$$

when m and n are both odd, while $\sigma_{nm} = 0$ otherwise. In addition to $\mathcal{A}$, the result (51) for the eigenvalues depends on the ratio a/b. This is an example of a feature of the result anticipated at the end of Sec. II.

Results for Re Φ and Im Φ for this geometry are shown in Figs. 4–7 for $\gamma = 7/5$ and for $\mathcal{A} = 1.1$, 2, and 11 and $a/b = 0.1$ and 1. The results for $\mathcal{A}$ close to 1 coincide with those given in Fig. 2. Notice also that the formulas are invariant under an interchange of a and b, so that it is sufficient to consider $a \leq b$.

The graphs are similar to those of the previous case and the same comments apply.

V. VISCOUS DISSIPATION

For a spherical bubble in an unbounded liquid, viscosity only affects the condition of balance of normal stresses and is usually of little importance unless the bubble radius is small. The present situation is different due to the viscous dissipation of energy in the course of the motion of the two liquid columns bounding the bubble. The effect can be estimated as follows (Oğuz and Prosperetti, 1998).

With the approximation of parallel flow, the viscous energy dissipation per period for the jth liquid column ($j = 1,2$) is

$$\mathcal{E}_j = \frac{\nu m_j}{S} \int_0^{2\pi/\omega} dt \int_S dS \left(\frac{\partial u}{\partial r} \right)^2, \tag{53}$$

where ν is the kinematic viscosity coefficient, $m_j = \rho S L_j$ is the mass of liquid constituting the column, and u is the axial velocity. For a harmonic oscillator with velocity $\dot{x}_j$ and damping parameter β_{vj}, the energy dissipated in a cycle is

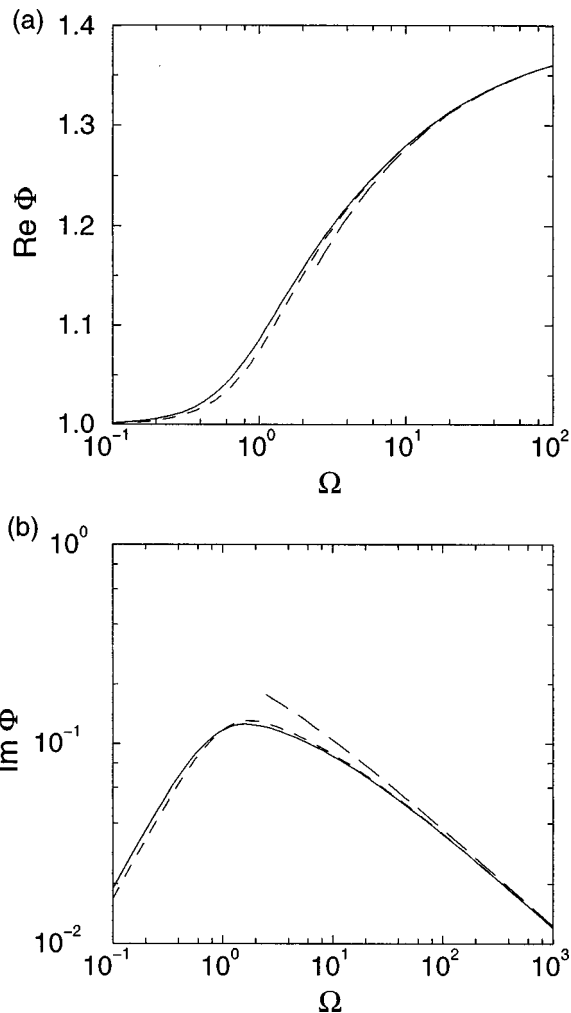$$\mathcal{E}_{dj} = 2\beta_{vj} \int_0^{2\pi/\omega} \dot{x}_j^2 \, dt. \tag{54}$$

FIG. 4. The real (a) and imaginary (b) parts of Φ as functions of the dimensionless frequency Ω defined in (19) for $\gamma = 7/5$ for a rectangular cross section. The bubble aspect ratio $\mathcal{A}$ is 2 and the lines are for $a/b = 1$ (solid) and 0.1 (dashes). The interrupted line marked with long dashes is the asymptotic approximation (39) valid at high frequencies.

Upon equating (53) and (54) one can define an equivalent viscous damping parameter by

$$\beta_{vj} = \frac{\omega \nu m_j}{2\pi S} \int_0^{2\pi/\omega} dt \int_S dS \left[\frac{\partial}{\partial r} \left(\frac{u}{\dot{x}_j} \right) \right]^2. \tag{55}$$

A relation between u and $\dot{x}_j$ can be established by equating the volume flow rates:

$$S\dot{x}_j = \int_S u \, dS. \tag{56}$$

From the linearity of this relation it is clear that the integral in (55) will be independent of $\dot{x}_j$. Note that, from (55), we see that

$$b_v = \frac{\beta_{v1}}{m_1} = \frac{\beta_{v2}}{m_2}. \tag{57}$$

An exact solution of the Navier–Stokes equation for parallel oscillatory flow in an infinitely long circular tube is available (see, e.g., Leal, 1992), but it is expressed in terms of Bessel functions and the integral in (55) cannot be evalu-
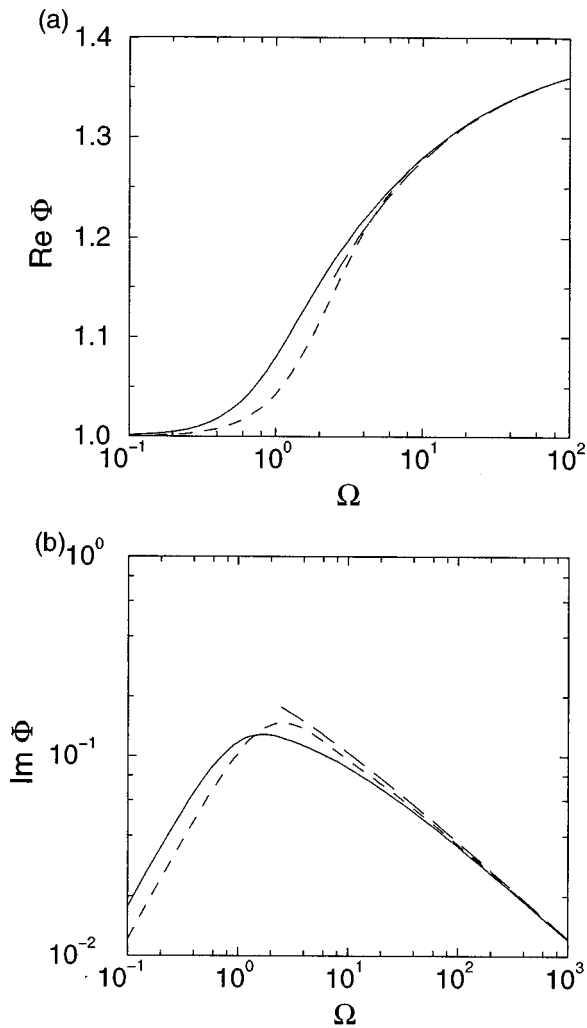
FIG. 5. The real (a) and imaginary (b) parts of Φ as functions of the dimensionless frequency Ω defined in (19) for $\gamma = 7/5$ for a rectangular cross section. The bubble aspect ratio $\mathscr{A}$ is 11 and the lines are for $a/b = 1$ (solid) and 0.1 (dashes). The interrupted line marked with long dashes is the asymptotic approximation (39) valid at high frequencies.

FIG. 6. The real (a) and imaginary (b) parts of Φ as functions of the dimensionless frequency Ω defined in (19) for $\gamma = 7/5$ for a rectangular cross section with $a/b = 0.1$. The bubble aspect ratio $\mathscr{A}$ is 1.1 (dotted), 2 (solid), and 11 (short dashes). The interrupted line marked with long dashes is the asymptotic approximation (39) valid at high frequencies.

ated in closed form. By using the well-known result for Poiseuille flow one has the approximation

$$b_v = 4 \frac{\nu}{R^2}, \tag{58}$$

as also follows from the exact result (55) in the limit $\sqrt{\nu/\omega} \gg R$. In the opposite limit, $\sqrt{\nu/\omega} \ll R$, viscosity is only significant in a thin boundary layer at the tube wall and the corresponding result is

$$b_v = \sqrt{\frac{\pi \nu \omega}{2S}}. \tag{59}$$

The result has been written in this way to stress its applicability to tubes of arbitrary cross section, provided the viscous boundary layer thickness $\sqrt{\nu/\omega}$ is small compared with the shortest dimension of the cross section. In Fig. 8 we show the dimensionless viscous damping
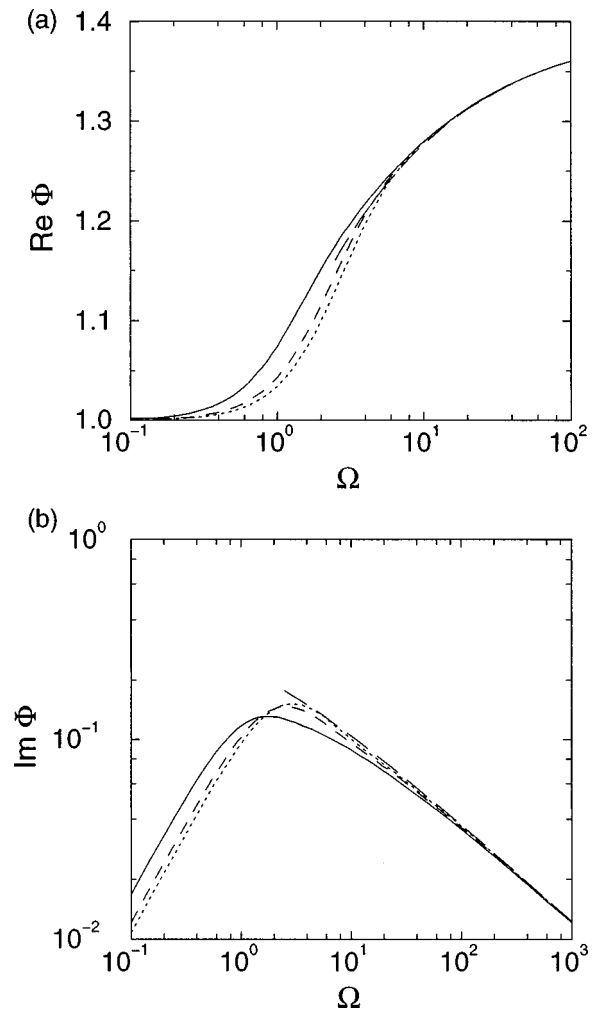
$$\tilde{b}_v = \frac{R^2 b_v}{4 \nu} \tag{60}$$

as a function of the Womersley number $\mathrm{Wo} = \omega R^2/\nu$ evaluated by numerical integration of the exact result (55), and we compare it with the two asymptotic limits (58) and (59) (dashed lines).

Upon introducing an equivalent damping in the equations of motion (4) and (5) along the lines outlined before, and again separating the real and imaginary parts of Φ as done in connection with Eq. (9), we have

$$m_1 \ddot{x}_1 + 2\beta_{v1} \dot{x}_1 - Sp_0 \Phi X = Sp_0 P_1, \tag{61}$$

$$m_2 \ddot{x}_2 + 2\beta_{v2} \dot{x}_2 + Sp_0 \Phi X = -Sp_0 P_2. \tag{62}$$

The steady solution of this system is given by

$$\frac{x_1 - x_{10}}{2L_B} = \frac{p_0}{2L_B \rho \Delta}$$

$$\times \left[\frac{P_1}{L_1} - \frac{P_1 - P_2}{L_1 + L_2} \frac{\omega_0^2}{\omega^2} \frac{1 + i \operatorname{Im} \Phi / \operatorname{Re} \Phi}{1 - 2ib_v/\omega} \right], \tag{63}$$
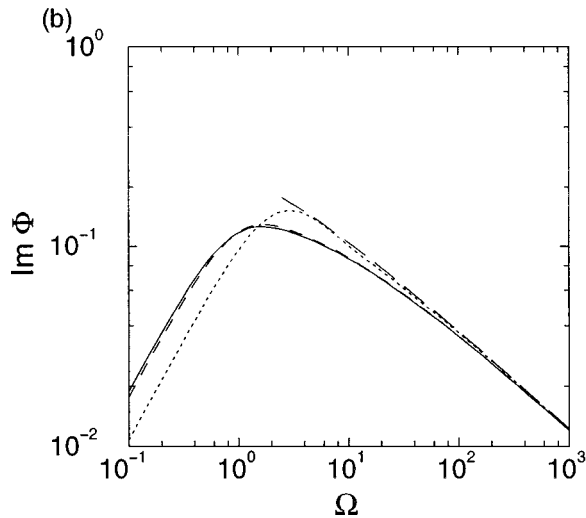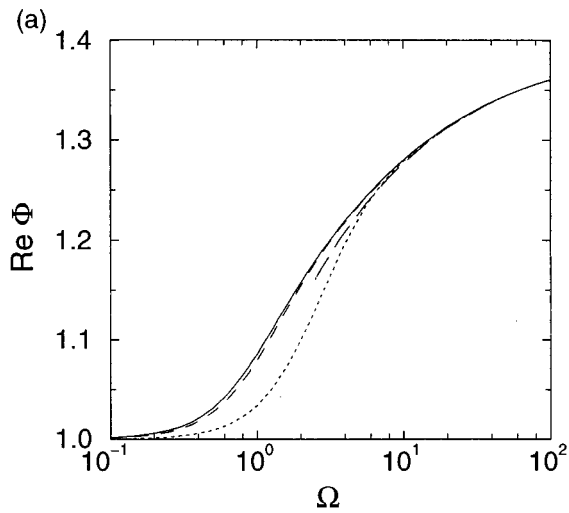
(a)

(b)

FIG. 7. The real (a) and imaginary (b) parts of Φ as functions of the dimensionless frequency Ω defined in (19) for $\gamma = 7/5$ for a square cross section, $a/b = 1$. The bubble aspect ratio $\mathscr{A}$ is 1.1 (dotted), 2 (solid), and 11 (short dashes). The interrupted line marked with long dashes is the asymptotic approximation (39) valid at high frequencies.
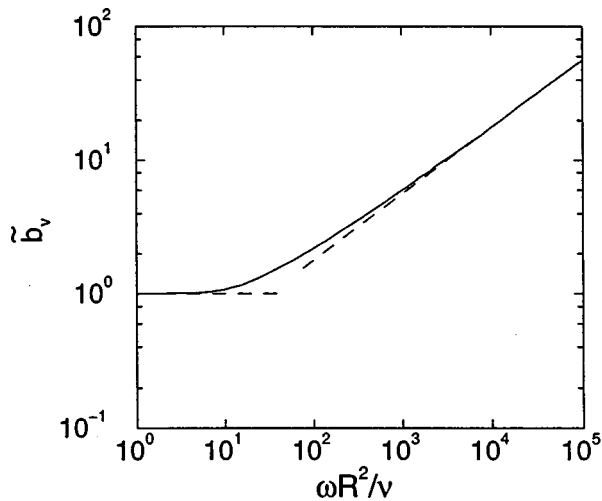

FIG. 8. The dimensionless viscous damping $\tilde{b}_v$ defined by (60) for a cylindrical tube according to the approximate procedure of Sec. V as a function of the Womersley number $\mathrm{Wo} = \omega R^2/\nu$.
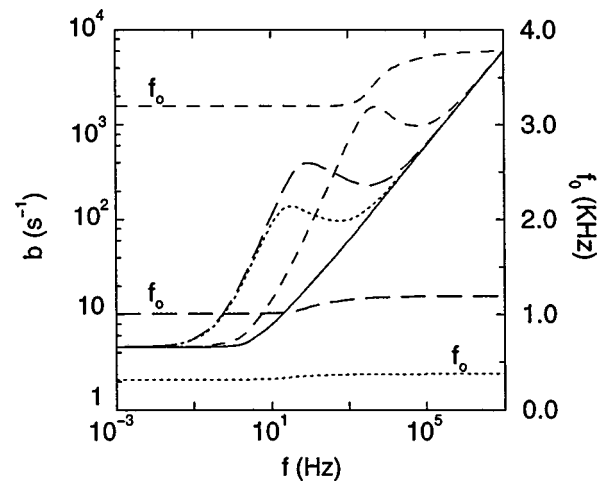

FIG. 9. Viscous and total damping (left scale) and resonance frequency f_0 (right scale) for an air bubble in a cylindrical tube with $R = 1$ mm and $L_1 = L_2 = 5$ mm as functions of the driving frequency f. The solid line is the viscous contribution to the damping. The dotted lines are for $2L_B = 10$ mm ($\mathscr{A} = 11$), the lines marked with long dashes for $2L_B = 1$ mm ($\mathscr{A} = 2$), and those with short dashes for $2L_B = 0.1$ mm ($\mathscr{A} = 1.1$). The liquid is water, the temperature 20 °C, and the undisturbed pressure atmospheric.

$$\frac{x_2 - x_{20}}{2L_B} = \frac{p_0}{2L_B \rho \Delta} \left[- \frac{P_2}{L_2} \right.$$

$$\left. - \frac{P_1 - P_2}{L_1 + L_2} \frac{\omega_0^2}{\omega^2} \frac{1 + i \ \mathrm{Im} \ \Phi/\mathrm{Re} \ \Phi}{1 - 2ib_v/\omega} \right], \quad (64)$$

from which, according to (1),

$$X = \frac{x_2 - x_{20}}{2L_B} - \frac{x_1 - x_{10}}{2L_B} = - \frac{p_0}{2L_B \rho \Delta} \left(\frac{P_1}{L_1} + \frac{P_2}{L_2} \right). \quad (65)$$
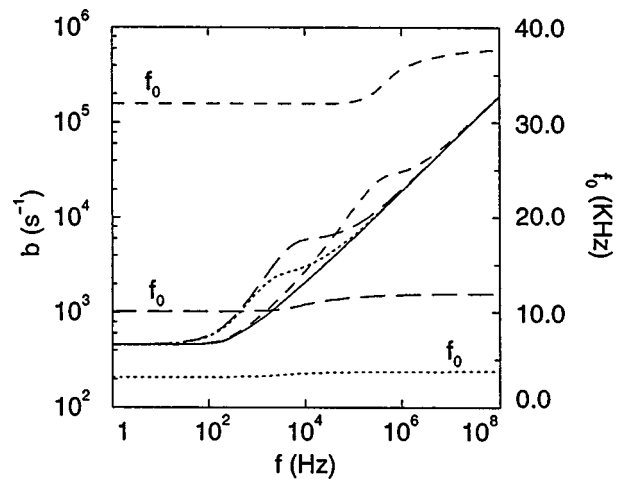
In these equations b_v is defined in (57),

FIG. 10. Viscous and total damping (left scale) and resonance frequency f_0 (right scale) for an air bubble in a cylindrical tube with $R = 0.1$ mm and $L_1 = L_2 = 0.5$ mm as functions of the driving frequency f. The solid line is the viscous contribution to the damping. The dotted lines are for $2L_B = 1$ mm ($\mathscr{A} = 11$), the lines marked with long dashes for $2L_B = 0.1$ mm ($\mathscr{A} = 2$), and those with short dashes lines for $2L_B = 0.01$ mm ($\mathscr{A} = 1.1$). The liquid is water, the temperature 20 °C, and the undisturbed pressure atmospheric.
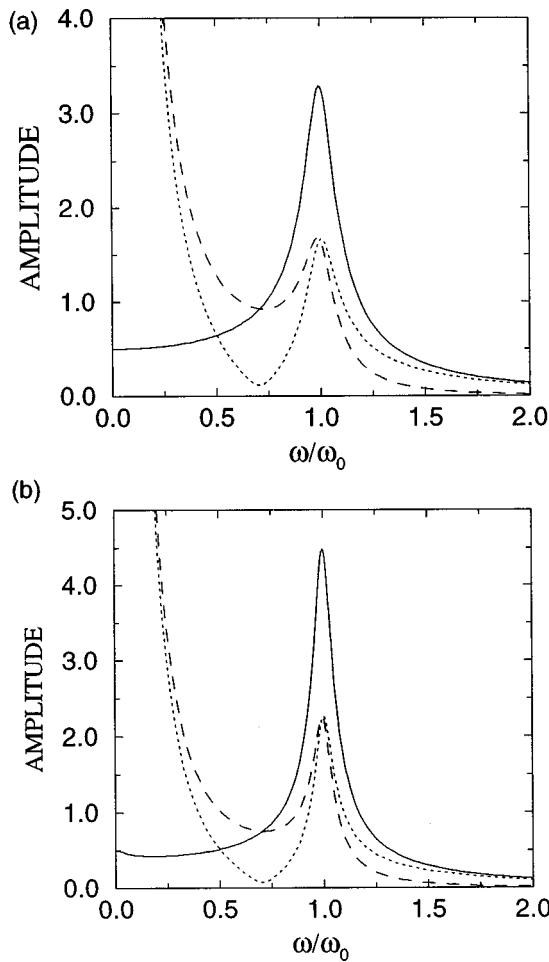
FIG. 11. Dimensionless amplitudes of oscillation of the left liquid surface $|(x_1-x_{10})/2L_BP_1|$ [dotted line, Eq. (63)], of the right surface $|(x_2-x_{20})/2L_BP_1|$ [dashes, Eq. (64)], and of the bubble length $|X/P_1|$, given by (65), as a function of the excitation frequency normalized by the resonance frequency. The bubble oscillation is driven by a pressure disturbance applied to the left liquid column. The tube radius is $R=1$ mm and the common length of the liquid columns 5 mm. Part (a) is for $2L_B=0.1$ mm ($\mathscr{A}=1.1$); this is the case shown by the line marked with short dashes in Fig. 9. Part (b) is for $2L_B=10$ mm ($\mathscr{A}=11$), which is the dotted line in Fig. 9. The gas is air, the liquid water, the temperature 20 °C, and the undisturbed pressure atmospheric.
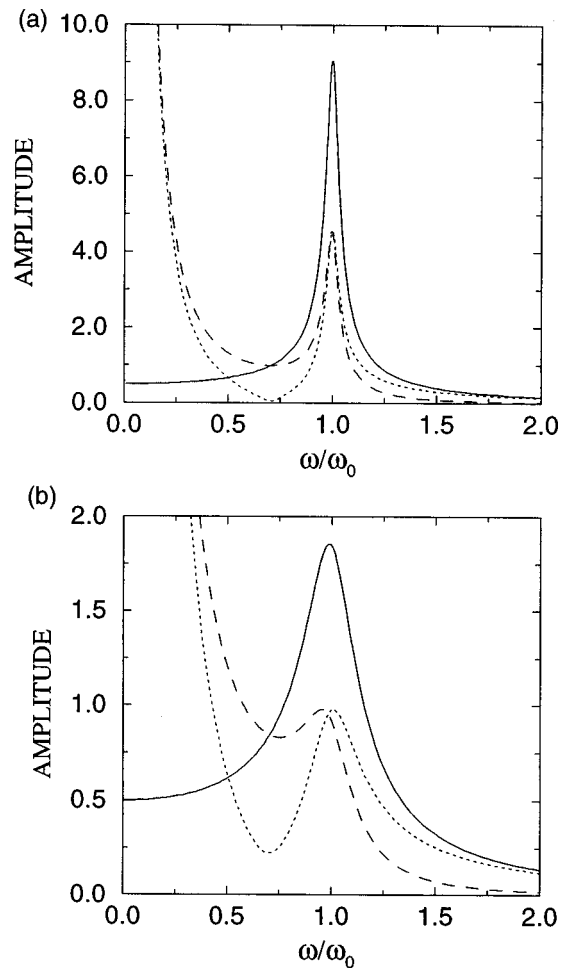

FIG. 12. Dimensionless amplitudes of oscillation of the left liquid surfaces $|(x_1-x_{10})/2L_BP_1|$ [dotted line, Eq. (63)], of the right surface $|(x_2-x_{20})/2L_BP_1|$ [dashes, Eq. (64)], and of the bubble length $|X/P_1|$, given by (65), as a function of the excitation frequency normalized by the resonance frequency. The bubble oscillation is driven by a pressure disturbance applied to the left liquid column. The tube radius is $R=0.1$ mm and the common length of the liquid columns 0.5 mm. Part (a) is for $2L_B=0.01$ mm ($\mathscr{A}=1.1$); this is the case shown by the line marked with short dashes in Fig. 10. Part (b) is for $2L_B=1$ mm ($\mathscr{A}=11$), which is the dotted line in Fig. 10. The gas is air, the liquid water, the temperature 20 °C, and the undisturbed pressure atmospheric.

$$\Delta = -\omega^2 + 2i\left(b_v + \frac{\omega_0^2}{2\omega}\frac{\text{Im }\Phi}{\text{Re }\Phi}\right)\omega + \omega_0^2, \tag{66}$$

and

$$\omega_0^2 = \frac{p_0}{2L_B\rho}\left(\frac{1}{L_1}+\frac{1}{L_2}\right)\text{Re }\Phi. \tag{67}$$

Since the present system has two degrees of freedom, we expect two characteristic frequencies. One corresponds to the center-of-mass motion which is subject to no restoring force. Resonance therefore occurs for $\omega=0$, as shown by the denominators in the last terms of (63) and (64). The resonance structure of the other mode is embodied in the quantity Δ defined in (66), from which we see that ω_0 is the resonant frequency while the total damping b, consisting of a viscous and a thermal part, is given by

$$b = b_v + \frac{\omega_0^2}{2\omega}\frac{\text{Im }\Phi}{\text{Re }\Phi}. \tag{68}$$

Figures 9 and 10 show graphs of b (left scale) and $f_0 = \omega_0/2\pi$ (right scale) as functions of the driving frequency $f=\omega/2\pi$ for several cases. The solid line is the viscous contribution (57). It is seen that thermal dissipation has a marked effect over a broad frequency range encompassing the resonant frequency.

In order to illustrate the nature of the solutions (63)–(65) we consider a situation in which the bubble is excited only on the left by a pressure P_1, while $P_2=0$. Figures 11 and 12 show $|(x_1-x_{10})/2L_BP_1|$, $|(x_2-x_{20})/2L_BP_1|$, and $|X/P_1|$, for several cases of Figs. 9 and 10. At very low frequencies the displacements of the two liquid columns are large, corresponding to the resonance at zero frequency mentioned before. The amplitude of oscillation of the bubble length, on the other hand, remains relatively small. As the

true resonance frequency is approached, the relative phase of the motion of the two liquid surfaces changes sign and, at resonance, the bubble elongation equals approximately twice the amplitude of oscillation of each surface. The sharpness of the resonance peak depends in a complex way on the values of the parameters. In general, it is found that, for a fixed bubble length and liquid columns of equal length, the peak becomes sharper the shorter the liquid column. When the left column is taken progressively longer than the right one, the peak decreases while the opposite trend is observed when the right column becomes progressively longer than the left one.

VI. SUMMARY AND CONCLUSIONS

We have studied the forced oscillations of a system composed of a gas bubble bounded by two liquid columns in a duct. It has been found that, while the natural frequency of the system is only weakly dependent on the thermal processes occurring in the gas, the damping parameter is very sensitive to the energy exchange between the gas and the surrounding surfaces. Even for tubes with a radius as small as 1 mm or less, thermal damping can be more significant than viscous damping over a broad frequency range.

The situation considered here is that of a bubble large enough to fill the cross section of the duct. Results for the resonance frequencies of smaller bubbles (without consideration, however, of thermal effects) are given in Oğuz and Prosperetti (1998).

ACKNOWLEDGMENTS

APPENDIX

Consider two eigenfunctions v_m, v_n satisfying (15) and homogeneous Dirichlet boundary conditions:

$$\nabla_\perp^2 v_m = -\frac{\lambda_m^2}{l^2} v_m, \quad \nabla_\perp^2 v_n = -\frac{\lambda_n^2}{l^2} v_n. \tag{A1}$$

Without loss of generality we take the eigenfunctions to be real. Multiply the first equation by v_n and the second one by v_m, subtract, and integrate over the cross section of the channel. The result is

$$\int (v_n \nabla_\perp^2 v_m - v_m \nabla_\perp^2 v_n)\, dS = -\frac{\lambda_m^2 - \lambda_n^2}{l^2} \int v_m v_n\, dS. \tag{A2}$$

By use of Green's identity and Stokes' theorem, it is readily shown that the left-hand side vanishes due to the vanishing of $v_{m,n}$ on the boundary. If the eigenvalues are distinct, this relation then implies that the integral on the right-hand side vanishes for $m \neq n$, i.e., that the eigenfunctions are orthogonal. If the eigenvalue is degenerate, the eigenfunctions spanning the corresponding eigenspace can be rendered orthogonal, e.g., by the Gram–Schmidt procedure. Hence we can assume that the eigenfunctions constitute an orthogonal system.

In order to prove (28), note that, as is readily verified, the σ_n's are exactly the coefficients of the expansion of the constant $1/\sqrt{S}$ over the basis of the v_n's:

$$\frac{1}{\sqrt{S}} = \sum_n \sigma_n v_n, \tag{A3}$$

provided the eigenfunctions are normalized to 1:

$$\int v_n^2\, dS = 1. \tag{A4}$$

Squaring (A3) and integrating over the cross section, by the orthogonality and normalization of the v_n's, we have

$$1 = \int_S \left(\frac{1}{\sqrt{S}}\right)^2 dS = \sum_n \sum_m \sigma_n \sigma_m \int_S v_n v_m\, dS = \sum_n \sigma_n^2. \tag{A5}$$

Apfel, R. E. (**1981**). ''Acoustic cativation,'' in *Methods of Experimental Physics*, edited by P. D. Edmonds (Academic, New York), Vol. 19, pp. 355–411.

Fujita, H., and Gabriel, K. J. (**1991**). ''New opportunities for micro actuators,'' in *Transducers '91* (IEEE, New York), pp. 14–20.

Graveson, P., Branebjerg, J., and Jensen, O. S. (**1993**). ''Microfluidics—A review,'' J. Micromech. Microeng. **3**, 168–182.

Leal, L. G. (**1992**). *Laminar Flow and Convective Transport Processes* (Butterworth-Heinemann, Boston).

Lin, L., and Pisano, A. P. (**1991**). ''Bubble forming on a micro line heater,'' in *Micromechanical Sensors, Actuators, and Systems* (ASME, New York), Vol. DSC-32, pp. 147–163.

Oğuz, H. N., and Prosperetti, A. (**1998**). ''The natural frequency of oscillation of gas bubbles in tubes,'' J. Acoust. Soc. Am. **103**, 3301–3308.

Plesset, M. S., and Prosperetti, A. (**1977**). ''Bubble dynamics and cavitation,'' Annu. Rev. Fluid Mech. **9**, 145–185.

Prosperetti, A. (**1984**). ''Bubble phenomena in sound fields: part one,'' Ultrasonics **22**, 69–77.

Prosperetti, A. (**1991**). ''The thermal behaviour of oscillating gas bubbles,'' J. Fluid Mech. **222**, 587–616.